Contrib Mineral Petrol (2005) 148: 707–720
DOI 10.1007/s00410-004-0631-x

ORIGINAL PAPER

D. E. Jacob · M. Bizimis · V. J. M. Salters

Lu–Hf and geochemical systematics of recycled ancient oceanic crust: evidence from Roberts Victor eclogites

Received: 8 July 2004 / Accepted: 13 October 2004 / Published online: 11 November 2004

Abstract Eclogites from the Roberts Victor mine, Kaapvaal craton are classic examples of subducted Achaean oceanic crust brought up as xenoliths by kimberlite. New in situ trace element and oxygen isotope data ($\delta^{18}O = 3.09$–$6.99‰$ SMOW) presented here reemphasise their origin from seawater-altered plagioclase-rich precursors. Their Hf–Nd isotopic compositions are not in agreement with compositions predicted by geochemical modelling of the isotopic composition of aged subducted oceanic crust. Instead, Hf isotopic compositions are very heterogeneous, varying between 0.281625 and 0.355077 (-37.8 and $+2561$ ε_{Hf}) at the time of kimberlite emplacement (128 Ma) in keeping with equally variable Nd isotopic compositions (0.511124–0.545092; -26.3 to $+636$ ε_{Nd}). However, most samples plot on the terrestrial array. The isotopic compositions of some samples are too extreme to play a major role in mixed peridotite-eclogite melting in basalt source regions, whereas the isotopic composition of other samples is reconcilable with a contribution of up to ca. 15% of eclogite partial melt to the MORB source. Most importantly, our results show that ancient subducted oceanic crust is not isotopically homogeneous and should not be treated as a ''component'' or ''reservoir'' during geochemical modelling. The heterogeneity reflects radiogenic in-growth starting from small compositional heterogeneities in gabbroic protoliths, followed by modification during sea-floor alteration, subduction and emplacement into the subcratonic lithosphere.

Editorial Responsibility: J. Hoefs

D. E. Jacob (✉)
Institut für Geowissenschaften, Universität Mainz,
Becherweg 21, D-55099 Mainz, Germany
E-mail: jacobd@uni-mainz.de

M. Bizimis · V. J. M. Salters
NHMFL and Department of Geology, Florida State University,
1800 E Paul Dirac Drive, Tallahassee, FL 32306, USA

M. Bizimis
Department of Earth Sciences, Florida International University,
Miami, FL 33199, USA

Introduction

Eclogitic and pyroxenitic lithologies in the Earth's mantle are receiving increased attention, due to their potential role in the formation of mid-ocean ridge and ocean island basalts (MORB, OIB: e.g. Salters and Hart 1989; Hirschmann and Stolper 1996; Lassiter and Hauri 1998; Stracke et al. 1999; Salters and Dick 2002; Pertermann and Hirschmann 2003b). Their mineralogy and comparatively enriched composition can satisfy the prerequisites of a number of models that explain the detailed major, trace element and isotopic characteristic of MORB and OIB as products of a mixed peridotitic-eclogitic/pyroxenitic source. Eclogites and pyroxenites in the Earth's mantle are readily available sources for melts at upper mantle P and T as a result of their mostly lower solidi compared to those of peridotite (e.g. Kornprobst 1970; Irving 1974; Pertermann and Hirschmann 2003a) and they provide garnet-bearing mineralogies within the spinel-peridotite stability field, allowing for a ''residual-garnet'' signature during shallow melting (e.g. Hirschmann and Stolper 1996). Because of this potential petrogenetic significance, it is important to characterise eclogites and pyroxenites geochemically in more detail in order to put better constraints on petrogenetic models.

Here, we present the first Lu–Hf isotopic data, as well as new major, trace element, other radiogenic (Rb–Sr, Sm–Nd) and stable isotope data on a suite of eclogitic xenoliths from the lithospheric mantle beneath the Roberts Victor kimberlite pipe, Kaapvaal craton, South Africa. Eclogite xenoliths from this kimberlite pipe were among the first for which an origin from subducted ancient oceanic crust was proposed (Jagoutz et al. 1984; MacGregor and Manton 1986). This interpretation has been extended to a number of eclogite suites from kimberlites worldwide over the years (Jacob 2004), but

Roberts Victor remains the "type-locality" of subducted Achaean oceanic crust, as the abundance and variability of eclogites there specifically enabled detailed study. The ancient oceanic crust model is based on two main lines of evidence, both of which exclude derivation of eclogite xenoliths as high-pressure cumulates or melts from the Earth's mantle (Jacob 2004). First, oxygen isotopic values worldwide deviate from those of the unchanged mantle, but are similar to the variation found in modern and ancient oceanic crust. This variation cannot be generated at depth (Clayton et al. 1975), but requires surface or near-surface hydrothermal processes, just like those operating in rifted modern oceanic crust. Second, half of all eclogite xenoliths from kimberlites have garnets with trace element patterns showing positive Eu-anomalies and flat heavy rare earth element (HREE) patterns that are unlike the usual high HREE abundance patterns of garnet from high-pressure rocks caused by mineral-melt partitioning characteristics (e.g. Johnson 1998). These anomalies are also visible in reconstructed eclogite bulk composition, and are often accompanied by positive Sr anomalies, indicating a plagioclase-bearing protolith (gabbro, troctolite) in which prograde metamorphic reactions formed garnet at the expense of plagioclase.

Samples and analytical methods

Eclogites are among the xenoliths sampled by many kimberlites. The Cretaceous Roberts Victor kimberlite (128 Ma, Smith et al. 1985) Orange Free State, South Africa, however, is exceptional in that eclogites make up more than 90% of its xenolith suite. Four of the six samples chosen for this study were previously studied, whereas two are newly collected samples (DEJ5, RV1) of bimineralic (cpx-garnet ± rutile) eclogite. All samples in this study are relatively large (> 10 cm to ca. 50 cm); four samples contain accessory rutile as exsolved needles in garnet and cpx or as discrete grains, one sample is diamond-bearing (RV1), one contains diamond and graphite (HRV247) and two samples contain coesite (DEJ5, BD1191). All samples are very coarse-grained with several millimetre large garnet and clinopyroxene grains. As is typical for cratonic eclogite xenoliths (Jacob 2004), both phases are clear and free of inclusions, verified both by visual inspection and by element scans with the electron microprobe. Modal proportions of cpx and garnet vary between 30:70 and 60:40 and mineral modes are given in Table 4. Sample HRV247 is a petrographically and compositionally layered diamond- and graphite-bearing eclogite (Hatton and Gurney 1979). However, all data for this sample presented here and those compiled from the literature are from one part of this xenolith and are therefore internally consistent. (For example, differences between Sm and Nd concentrations measured by isotope dilution (Smith et al. 1989: Table 5), laser-ablation ICP-MS (Table 2) and ion microprobe (Harte and Kirkley 1997) are less than 15%; Sm/Nd ratios are identical.)

Major element compositions for samples BD3699 and DEJ5 were determined with a JEOL JXA 8900 RL microprobe at the University of Göttingen following standard methods. On average, three spots per grain and five grains each of cpx and garnets were analysed; zonation was not detected. Major element compositions for other samples are taken from Hatton (1978: BD1175, BD1191), from Harte and Kirkley (1997: HRV247) and from Fett (1995: RV1) and are listed in Table 1. Oxygen isotopic compositions of garnet and cpx (Table 1) were obtained by the Laser-Fluorination method at Royal Holloway, University of London following methods described in Mattey et al. (1994) and are reported relative to SMOW. The total analytical uncertainty given for the $\delta^{18}O$-values are based on two to three replicate analyses of samples with weights ranging between 1.5 and 1.8 mg; the external reproducibility of the SC1OL standard was 0.1‰ during the course of the analyses.

Trace elements given in Table 2 were analysed by laser ablation microprobe (LAM) at the Department of Earth Sciences, Memorial University of Newfoundland, using a frequency-quadrupled 266 nm wavelength Nd:YAG laser integrated with an enhanced sensitivity Fisons PQII + "S" ICPMS (Günther et al. 1996). Analyses were performed on polished thin sections. Calcium concentrations in garnet and clinopyroxene determined by microprobe were used as internal standards for the ICPMS measurements, and titanium determined by electron microprobe was used as internal standard for rutiles (Table 3). NIST SRM 612 glass, doped with approximately 40 ppm of a large range of trace elements, was used as the external standard and BCR-2G as the secondary standard. Further details of the analytical procedures, data reduction and calculation of detection limits are given in Longerich et al. (1996).

Chemical separation of Hf and Lu and measurement of Hf isotopic compositions as well as of Lu and Hf concentrations were carried out at the Division of Isotope Geochemistry, NHMFL/FSU on whole rock powders as well as on high-purity mineral separates. 100% pure mineral separates were obtained by handpicking under the microscope followed by extensive leaching similar to procedures described by Jacob et al. (1994), and purity was confirmed by inspection under the microscope after leaching. Hafnium separations were performed either with the method described by Salters (1994, modified after Bizimis et al. 2003) or the method described by Munker et al. (2001), with the addition of an extra step for the further purification of Hf from Zr. Hafnium isotope measurements we performed by Hot-SIMS technique on the Lamont ISOLAB (Salters 1994; Bizimis et al. 2003). During the course of this study the JMC Hf standard was measured at 0.282199 ± 22 ($n = 15$) and all Hf isotope measurements in Table 5 are reported relative to the accepted JMC value of 0.28216. Lu/Hf ratios where determined with the techniques described by Bizimis et al. (2003, 2004). Neodymium and strontium isotopic compositions and concentrations were measured at the Division of Isotope Geochemistry,

Table 1 Major element and oxygen isotopic composition of garnets and clinopyroxenes from eclogite xenoliths

	BD 1191 gt[a]	BD 1191cpx[a]	BD 1175 gt[a]	BD 1175 cpx[a]	BD 3699 gt	BD 3699 cpx	RV 1 gt[b]	RV 1 cpx[b]	DEJ 5 gt	DEJ 5 cpx	HRV 247 gt[a]	HRV 247 cpx[a]
SiO_2	39.40	54.20	40.40	55.30	40.18	55.66	42.30	55.31	39.87	53.80	40.77	55.83
TiO_2	0.170	0.210	0.120	0.200	0.198	0.369	0.390	0.350	0.140	0.325	0.400	0.290
Al_2O_3	22.50	10.50	23.10	9.26	22.35	14.37	22.84	3.49	22.48	9.02	23.31	6.42
Cr_2O_3	0.04	0.050	0.25	0.320	0.08	0.097	0.22	0.180	0.10	0.095	0.00	0
FeO	18.19	5.55	11.67	2.32	14.65	2.47	11.06	3.62	18.95	5.59	11.26	2.61
MnO	0.410	0.040	0.220	0	0.266	0.023	0.360	0.090	0.396	0.054	0.250	0
MgO	10.30	9.14	15.50	11.50	11.82	7.43	19.46	16.02	10.01	9.71	14.98	13.37
CaO	8.89	14.10	7.88	16.00	10.43	11.37	3.70	18.05	8.79	15.54	9.03	18.59
Na_2O	0.05	5.76	0.05	4.95	0.06	6.96	0.09	2.20	0.04	5.02	0.12	3.37
K_2O	0	0	0	0.070	0	0.299	0	0.280	0	0.001	0	0.070
Total	100.0	99.6	99.2	99.9	100.0	99.1	100.0	99.6	100.8	99.2	100.1	100.6
Si	2.956	1.947	2.951	1.966	2.973	1.984	3.011	1.997	2.976	1.950	2.954	1.989
Ti	0.010	0.006	0.007	0.005	0.011	0.010	0.021	0.010	0.008	0.009	0.022	0.008
Al	1.990	0.445	1.989	0.388	1.949	0.604	1.916	0.149	1.978	0.385	1.991	0.270
Cr	0.002	0.001	0.014	0.009	0.005	0.003	0.012	0.005	0.006	0.003	0.000	0
Fe	1.141	0.167	0.713	0.069	0.907	0.074	0.658	0.109	1.183	0.169	0.682	0.078
Mn	0.026	0.001	0.014	0	0.017	0.001	0.022	0.003	0.025	0.002	0.015	0
Mg	1.152	0.490	1.688	0.609	1.304	0.395	2.065	0.862	1.114	0.525	1.618	0.710
Ca	0.715	0.543	0.617	0.609	0.827	0.434	0.282	0.698	0.703	0.604	0.701	0.710
Na	0.007	0.401	0.007	0.341	0.008	0.481	0.012	0.154	0.006	0.352	0.017	0.233
K	0	0	0	0.003	0	0.014	0	0.013	0	0	0	0.003
$\delta^{18}O$	3.09 ±0.01	3.45 ±0.02	6.00 ±0.02	6.13 ±0.03	6.48 ±0.01	6.99 ±0.01	6.75 ±0.02	6.99 ±0.03	3.43 ±0.01	3.41 ±0.02	5.93 ±0.02[c]	6.14 ±0.02[c]

[a]Data from Hatton (1978)
[b]Data from Fett (1995)
[c]D. Lowry, personal communication 1999

Table 2 Trace element concentrations of garnets and clinopyroxenes measured by Laser ablation ICP-MS

	BD1191 gt	BD 1191 cpx	BD 1175 gt	BD 1175 cpx	BD 3699 gt	BD 3699 cpx	RV1 gt	RV 1 cpx	DEJ 5 gt	DEJ 5 cpx
	$n=3$	$n=3$	$n=3$	$n=3$	$n=6$	$n=4$	$n=4$	$n=3$	$n=5$	$n=5$
Ba	<0.03	0.03	<0.01	0.18	0.04	0.09	<0.15	8.15	0.029	0.108
Rb	<0.03	<0.02	<0.02	<0.03	<0.02	<0.06	<0.1	<0.1	0.092	0.045
Th	<0.01	<0.01	<0.01	0.1	<0.01	<0.01	0.036	0.424	0.013	0.021
U	<0.01	<0.01	0.02	0.02	0.015	<0.01	0.017	0.030	<0.022	0.152
Nb	0.007	0.004	0.02	0.03	<0.04	0.02	0.020	0.020	0.025	0.006
Ta	<0.004	<0.01	<0.004	<0.004	<0.01	<0.01	<0.01	<0.01	0.004	<0.005
La	<0.01	0.002	0.025	2.45	0.025	0.729	0.035	15.6	0.004	0.015
Ce	0.007	0.015	0.380	9.09	0.345	2.72	0.524	47.0	0.023	0.107
Pr	0.006	0.013	0.1577	1.50	0.161	0.488	0.150	6.13	0.027	0.068
Sr	0.112	16.5	1.12	470	0.678	206	1.16	765	0.116	29.1
Nd	0.132	0.246	1.53	5.95	1.78	2.63	1.14	21.7	0.474	0.846
Sm	0.681	0.283	0.947	0.797	1.23	0.661	0.981	3.74	1.29	0.640
Zr	2.05	3.47	7.34	10.4	7.82	43.3	57.7	33.7	5.27	6.75
Hf	0.09	0.400	0.133	0.64	0.165	2.22	1.12	1.67	0.193	0.509
Eu	0.582	0.155	0.550	0.277	0.675	0.196	0.526	1.12	0.827	0.239
Ti	1020	1259	719	1199	1187	2212	2338	2098	839	1948
Gd	3.03	0.441	1.14	0.323	1.29	0.367	1.97	2.39	4.90	0.538
Tb	0.958	0.074	0.205	0.032	0.245	0.035	0.495	0.341	1.14	0.077
Dy	8.44	0.368	1.24	0.103	1.56	0.141	3.67	1.23	9.08	0.371
Y	57.5	1.42	6.42	0.310	8.39	0.454	23.4	4.60	55.8	1.08
Ho	2.42	0.068	0.267	0.014	0.337	0.019	0.855	0.179	2.44	0.049
Er	7.70	0.126	0.749	0.021	1.00	0.037	2.88	0.341	7.00	0.113
Tm	1.29	0.013	0.123	<0.01	0.16	<0.01	0.423	0.034	1.10	0.014
Yb	9.40	0.086	0.841	0.010	1.04	0.025	3.23	0.183	8.19	0.074
Lu	1.56	0.009	0.133	<0.05	0.165	0.002	0.542	0.027	1.17	0.008
Sc	63.0	19.0	37.0	11.0	47.2	9.33	69.8	16.7	56.0	14.0
V	n.m.	n.m.	n.m.	n.m.	n.m.	n.m.	154	252	n.m.	n.m.
Cr	256	231	1182	1704	331	590	866	391	412	482
Ni	24.0	253	59.0	526	43.7	363	21.0	109	19.9	304
Cu	6.00	44	6.00	8.00	5.75	15.7	6.00	5.74	n.m.	n.m.
Zn	72.0	49.0	64.0	49.0	87.7	67.3	55.0	49.7	n.m.	n.m.
Ga	n.m.	n.m.	n.m.	n.m.	n.m.	n.m.	14.0	8.03	n.m.	n.m.
Co	n.m.	n.m.	n.m.	n.m.	n.m.	n.m.	21.9	53.6	56.9	32.2

n.m. not measured

Table 3 Trace element concentrations (in ppm) of rutiles measured by Laser ablation ICP-MS. TiO_2 determined by electron microprobe

	BD 1191	BD 1175-1	BD 1175-2	BD 1175-3
TiO_2	98.9 wt%	96.62 wt%	96.62 wt%	96.62 wt%
Ba	< 0.12	0.19	< 0.12	< 0.21
Th	< 0.06	< 0.13	< 0.13	< 0.01
U	< 0.35	0.22	0.22	0.15
Nb	< 1.67	94.1	101	88.1
Ta	< 0.3	27.3	29.0	23.9
Zr	285	3.319	3.552	3.446
Hf	17.8	96.7	107.0	100.5
Lu	0.623	0.09	0.06	0.047
Cr	< 736	1.099	1.166	1.326
Ni	< 199	< 28	64	98

NHMFL/FSU, Tallahassee, USA, and are given in Table 5. Measurements were carried out on a Finnigan MAT 262 multicollector mass spectrometer. Neodymium was measured as metal and normalised to $^{146}Nd/^{144}Nd = 0.7219$; Sr was normalised to $^{86}Sr/^{88}Sr = 0.1194$. The standard values obtained at NHMFL/FSU were $^{143}Nd/^{144}Nd = 0.511846 \pm 16$ for the La Jolla Nd standard and 0.708006 ± 18 for the E & A standard. Laser ablation ICP-MS and isotope dilution results for Lu, Hf, Sm and Nd generally agree within 15%, and coherence of the two methods is limited by sample homogeneity rather than by analytical factors. For example, sample RV1 which exhibits variations in Sm and Nd between individual laser ablation analyses due to small grain to grain inhomogeneity also yields less reproducible isotope dilution results. Likewise, Hf concentration data are less reproducible for samples with rutile inclusions (DEJ5) than for rutile-free samples.

Secondary geochemical overprint and the necessity for reconstructed bulk compositions

All eclogite xenoliths from kimberlites show visual and geochemical signs of multiple secondary processes that can significantly alter the bulk eclogite composition. Most prominent changes are introduced by infiltrating kimberlitic magma (e.g. Barth et al. 2001); surface alteration and precipitates from groundwater have also been shown to affect mantle xenoliths (Berg 1968; Zindler and Jagoutz 1988), while mantle metasomatism can also leave its imprint on the xenolith's bulk chemistry (e.g. Dawson 1984). Infiltrating kimberlitic magma, for example, precipitates carbonates and other kimberlitic minerals along veins which are often readily visible in thin section. However, the magma also reacts with the primary eclogitic minerals forming new silicates (e.g. amphiboles, mica, cpx) and oxides (e.g. spinels, McCormick et al. 1994). To constrain the primary compositions of the xenoliths it is vital to recognize this fact and to bypass the geochemical overprint. A common method in kimberlitic xenolith studies is to reconstruct clean bulk compositions from mineral data and modal estimates. To emphasize the necessity of this approach we carried out trace element and Nd–Hf isotopic analyses on acid-leached and unleached bulk eclogite powders. The results, summarized in the Appendix, show that although some of the foreign components are leachable, the leached eclogite residues are isotopically similar to the kimberlite. This reflects that major components of the secondary mineral paragenesis formed by reaction with the kimberlitic magma are not leachable.

Table 4 Calculated bulk major, trace element and oxygen isotopic compositions based on the modal mineralogy given

	BD 1191	BD 1175	BD 3699	RV 1	DEJ 5	HRV 247
SiO_2	46.80	49.64	48.07	48.81	48.23	45.59
TiO_2	0.190	0.170	0.285	0.370	0.251	0.365
Al_2O_3	16.50	14.52	18.28	13.17	14.40	17.91
Cr_2O_3	0.045	0.293	0.088	0.200	0.096	0
FeO	11.87	5.87	8.44	7.34	10.93	8.49
MnO	0.225	0.084	0.142	0.225	0.191	0.170
MgO	9.72	13.02	9.58	17.74	9.83	14.46
CaO	11.50	12.91	10.91	10.88	12.84	12.09
Na_2O	2.91	3.09	3.58	1.15	3.03	1.16
K_2O	0	0.043	0.154	0.140	0.002	0.02
Total	99.8	99.6	99.6	99.8	99.8	100.3
Mg#	59	80	67	81	62	75
T (°C) 5.0 GPa	1178	1033	1099	1094	1117	1049
$\delta^{18}O$	3.27	6.08	6.74	6.87	3.42	6.00
%gt	50	38	49	50	60	68
%cpx	50	62	51	50	40	32
other	rut (n)	rut (d)	–	rut (d), di	rut (n)	graph, di
Ba	< 0.03	0.112	0.0655	4.08	0.061	
Rb	< 0.02	< 0.03	< 0.06	< 0.1	0.073	
Th	< 0.01	0.062	< 0.01	0.230	0.016	
U	< 0.01	0.020	< 0.01	0.024	0.061	
Nb	0.005	0.026	0.010	0.02	0.018	
Ta	< 0.01	< 0.004	< 0.01	< 0.01	< 0.005	
La	< 0.002	1.53	0.384	7.83	0.012	
Ce	0.01	5.78	1.55	23.8	0.067	
Pr	0.01	0.992	0.327	3.14	0.066	
Sr	8.32	292	105	383	11.7	
Nd	0.189	4.27	2.21	11.4	0.62	
Sm	0.482	0.854	0.938	2.36	1.03	
Zr	2.76	9.22	25.9	45.7	5.86	
Hf	0.245	0.447	1.21	1.39	0.319	
Eu	0.369	0.381	0.431	0.825	0.592	
Ti	1.140	1.017	1.710	2.218	1.283	
Gd	1.74	0.635	0.817	2.18	3.16	
Tb	0.516	0.098	0.138	0.418	0.714	
Dy	4.40	0.534	0.838	2.45	5.60	
Y	29.5	2.63	4.34	14.0	33.9	
Ho	1.25	0.110	0.175	0.517	1.49	
Er	3.91	0.297	0.510	1.61	4.24	
Tm	0.654	0.047	0.078	0.228	0.666	
Yb	4.74	0.325	0.520	1.70	4.94	
Lu	0.784	0.050	0.082	0.284	0.702	
Sc	41	20.9	27.9	43.2	39.2	
V				203		
Cr	244	1.506	463	629	440	
Ni	139	349	207	65.2	134	
Cu	25	7.24	10.8	5.87		
Zn	60.5	54.7	77.3	52.3		
Ga				11.0		
Co				37.8	47.0	

Accessories: *rut (n)* rutile needles in silicates, *rut (d)* discrete rutile grains, *di* diamond, *graph* graphite

Table 5 Isotopic data and trace element concentrations for eclogitic minerals measured by isotope dilution

	BD 1191 gt	BD 1191 cpx	BD 1175 gt	BD 1175 cpx	BD 3699 gt	BD 3699 cpx	RV 1 gt	RV 1 cpx	DEJ 5 gt	DEJ 5 cpx	HRV 247 cpx	HRV 247 gt
$^{176}Hf/^{177}Hf$	0.361708	0.288413	0.283145	0.281978	0.281697	0.281500	0.282157	0.281907	0.306277	0.282286	0.282665	0.282915
2σ	0.000025	0.000036	0.000054	0.000018	0.000013	0.000019	0.000014	0.000012	0.000027	0.000013	0.000027	0.000020
$^{176}Hf/^{177}Hf_i$	0.355077	0.288406	0.282843	0.281977	0.281625	0.281500	0.281991	0.281901	0.304905	0.282264	0.282663	0.282772
$^{176}Lu/^{177}Hf$	2.767	0.003	0.1259	0.00022	0.0301	0.00010	0.0693	0.0023	0.573	0.0092	0.00051	0.05972
$^{143}Nd/^{144}Nd$	0.54769[a]	0.53358[a]	0.51193[a]	0.51152[a]	0.51554[a]	0.51530[a]	0.511492	0.511494	0.529580	0.520292	0.51196[b]	0.51225[b]
2σ	0.00004	0.00006	0.00004	0.00006	0.00002	0.00002	0.000008	0.000012	0.000014	0.000020	0.00002	0.00002
$^{143}Nd/^{144}Nd_i$	0.545092	0.532968	0.511638	0.511465	0.515143	0.515182	0.511124	0.511406	0.528204	0.519909	0.51189	0.51192
$^{147}Sm/^{144}Nd$	3.102	0.7306	0.3489	0.0659	0.4737	0.1412	0.4393	0.1056	1.643	0.4577	0.086	0.390
$^{87}Sr/^{86}Sr$	n.m.	0.70091	0.703465	0.70155[a]	0.703373	0.703350[a]	0.704249	0.703658	0.704783	0.700913	0.70593[b]	0.70615[b]
2σ		Not given	0.000015	Not given	0.000012	Not given	0.00001	0.00002	0.000014	0.00001	0.00002	0.00006
$^{87}Sr/^{86}Sr_i$		*0.700904*	*0.703377*	*0.701550*	*0.703229*	*0.703349*	*0.703914*	*0.703657*	*0.700888*	*0.700905*	0.70593	0.70614
$^{87}Rb/^{86}Sr$	*0.7343*	*0.0033*	*0.0481*	*0.0002*	*0.0794*	*0.0003*	*0.185*	*0.0004*	*2.141*	*0.0042*	0.0001	0.007
εHf_i	2561	202	5.4	−25.3	−37.8	−42.2	−24.8	−28.0	786	−15.1	−1.0	2.8
εNd_i	636	400	−16.3	−19.7	52.1	52.9	−26.3	−20.8	307	145	−11.4	−10.8
Rb (ppm)	n.m.	n.m.	n.m.	n.m.	n.m.	n.m.	n.m.	n.m.	n.m.	n.m.	0.01[b]	0.002[b]
Sr (ppm)	n.m.	n.m.	n.m.	n.m.	n.m.	n.m.	n.m.	n.m.	n.m.	n.m.	280[b]	0.78[b]
Nd (ppm)	0.114	0.211	1.438	6.931	3.586	2.748	1.35	25.7	n.m.	n.m.	7.80[b]	1.687[b]
Sm (ppm)	0.585	0.255	0.830	0.756	2.810	0.642	0.983	4.49	n.m.	n.m.	1.11[b]	1.089[b]
Hf (ppm)	0.4072[c]	0.0676[c]	0.148	0.639	1.408	2.235	1.03	2.24	0.249[c]	0.802	1.312	0.691
Lu (ppm)	1.3047	0.0086	0.130	0.001	0.296	0.0015	0.546	0.0269	0.996	0.0074	0.00469	0.2877

n.m. not measured

[a]Data compiled from Jagoutz et al. (1984)

[b]Data from Smith et al. (1989); calculation of $^{87}Rb/^{86}Sr$ and $^{87}Sr/^{86}Sr_i$ in italics is based on data from Tables 2 and 3 (i.e. maximum concentrations of Rb). $^{87}Rb/^{86}Sr$ ratios are therefore maximum values and $^{87}Sr/^{86}Sr_i$ ratios are minimum values

[c]Data are corrected for blank contribution. Initial Hf isotopic ratios are calculated with $\lambda = 1.87 \times 10^{-11}$

Clean whole rock compositions in terms of major and trace elements (Table 4) were reconstructed using mineral data and mineral modes. Eclogite xenoliths are typically coarse-grained and, since accurate mineral modes depend on sample size and homogeneity, errors can be as large as 20%. This suite of samples, however, consists of relatively large nodules (between ca. 10 and 50 cm) and modal estimations are therefore more precise (ca. within 10%). The amount of rutile, however, is more difficult to estimate. Barth et al. (2001) determined rutile abundances in eclogite xenoliths from West Africa by Ti mass balance to lie between 0.1 and 0.9 wt%. We determined the rutile content by mass balance using the Ti concentration in the solution ICP–MS analyses of whole rock powder and the Ti concentration of the reconstructed bulk silicate rock. The difference in Ti was assigned to rutile, yielding a maximum estimate for the weight percentage of TiO_2 in the eclogite, since kimberlite infiltration can increase the Ti content in eclogite by crystallization of secondary phases, such as Ti-bearing phlogopite. For the Roberts Victor suite, TiO_2 concentrations between 0 and 0.4 wt% (corresponding to 0 and 0.33% modal rutile) were calculated.

However, all samples show uniformly low Nb and Ta concentrations in their reconstructed bulk silicate composition. This is strong evidence that phases in all studied samples, irrespective of their current rutile contents, equilibrated with accessory rutile (Jacob and Foley 1999) and that rutile is not homogeneously distributed in the rock and therefore not always observed. If TiO_2 concentrations between 0.1 and 0.4 wt% are assumed for the whole rock reconstruction of all samples, irrespective of whether rutile was observed or not, this results in Ti abundances of about two to five times primitive mantle (Sun and McDonough 1989) creating slightly positive (BD1175, BD3699, BD1191) or no Ti anomalies at all (RV1, DEJ5) in the spidergrams. BD1175 and BD1191 show positive Nb anomalies when their bulks are calculated with 0.4% rutile. For comparison, rutile-bearing eclogite xenoliths from Koidu, Sierra Leone range between two and seven times primitive mantle in Ti abundances (Barth et al. 2001) and rutile-free eclogites from Udachnaya, Siberia, have bulk Ti abundances of two to three times primitive mantle (Jacob and Foley 1999). This is similar to Ti abundances in oceanic gabbros (one to five times PM, Bach et al. 2001), but lower than average modern MORB (seven times primitive mantle: $TiO_2 = 1.6$ wt%, Hofmann 1988).

Results

Major and trace elements

Major and trace element concentrations of clinopyroxenes and garnets are presented in Table 1. Garnets are pyrope-almandine-grossular solid solutions with 10–28 mol% grossular component, clinopyroxenes are diopside–hedenbergite–jadeite solid solutions with very small components of Tschermak's molecule and jadeite contents between 15 and 48 mol%. Based on the Na_2O-content of garnet, RV1 and HRV247 classify as Group I eclogites (i.e. with higher equilibration pressures than Group II), consistent with the occurrence of diamond in these samples; all other samples are Group II eclogites (McCandless and Gurney 1989). Temperature estimates using the thermometer based on Mg–Fe_{tot} exchange between cpx and garnet (Ellis and Green 1979) yield temperatures between 1,033 and 1,148°C at 5.0 GPa (Table 4), well within the range of temperatures observed for Roberts Victor eclogites at the same assumed pressure (Group I: 1,010–1,376°C, Group II: 820–1,376°C; Jacob 2004).

Three eclogite samples (BD1175, RV1, HRV247) have picritic compositions with reconstructed bulk MgO-contents >12 wt% and three are basaltic (BD1191, BD3699, DEJ5; Table 4). Reconstructed bulk Mg-numbers (100*Mg/(Mg + Fe)) range between 59 and 81, Na_2O-contents are between 1.10 and 3.58 wt% and fall within the range observed for eclogitic xenoliths from kimberlites worldwide that are interpreted to be oceanic crust (Jacob 2004), but are higher than the range of Na_2O-contents of eclogite suites thought to represent metamorphosed cumulates (e.g. Barth et al. 2002; Schmickler et al. 2004). Since quartz is seldom described in eclogite xenoliths, it was suggested that most have lost a tonalitic melt component upon subduction (e.g. Rudnick 1995; Jacob and Foley 1999). However, SiO_2-concentrations overlap with those of seawater-altered oceanic gabbros (Fig. 1), and, although melt-loss seems likely, it is difficult to constrain. If a realistic loss of 20% tonalitic component is assumed, the restored bulk eclogite compositions (using tonalitic melt No. 4 of Rapp and Watson 1995) become more basaltic with Mg-contents below 12 wt% (except for samples HRV247 and RV1); Mg-numbers drop in the range of 56–76 and Na_2O-contents increase (1.59–3.54 wt%). These compositions still overlap with those of the oceanic gabbros (Fig. 1).

Roberts Victor eclogites are well known for their large variation of $\delta^{18}O$-values (Ongley et al. 1987; Jacob 2004). This is reflected by the oxygen isotopic compositions of the samples in this study which range between 3.27 and 6.87‰ in reconstructed whole rocks. Two of the samples have $\delta^{18}O$-values lower than that of normal mantle (5.61 ± 0.31‰, Mattey et al. 1994); all other samples have higher $\delta^{18}O$-values. This range of $\delta^{18}O$ values can only be produced by surface processes involving seawater, similar to those operating in modern oceanic crust (e.g. Alt 1995) and is one of the key pieces of evidence for the oceanic crustal origin of eclogite xenoliths.

Clinopyroxenes in samples BD1191 and DEJ5 are very depleted in light rare earth elements (LREE, Fig. 2a, b), and coexisting garnets are more enriched in HREE than other samples of this suite. Such extreme depletions in LREE and enrichments in HREE are recorded only in eclogites from the Roberts Victor kimberlite (Jacob 2004). Clinopyroxenes in RV1 are more enriched in LREE and LILE than the majority of cpx

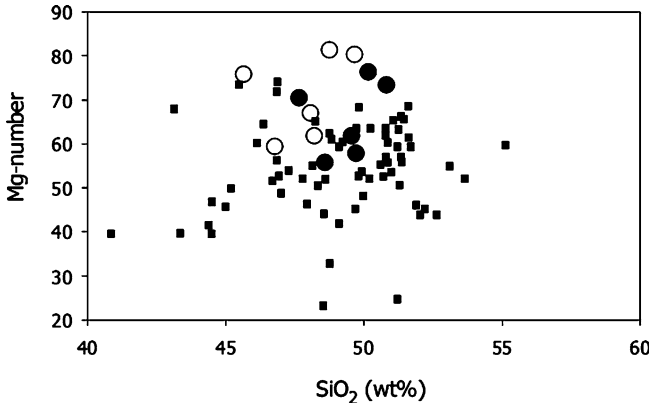

Fig. 1 Major element compositions of Roberts Victor eclogites (reconstructed from mineral data and mode, *solid circles*) compared with those of oceanic gabbros (*solid squares*: Zimmer et al. 1995; Hart et al. 1999; Bach et al. 2001). Addition of 20% tonalitic melt (Experiment No. 4, Rapp and Watson 1995) shifts the compositions towards higher SiO_2 and lower Mg-number (*open circles*). Mg-number = $Mg/(Mg+Fe_{tot})\times100$

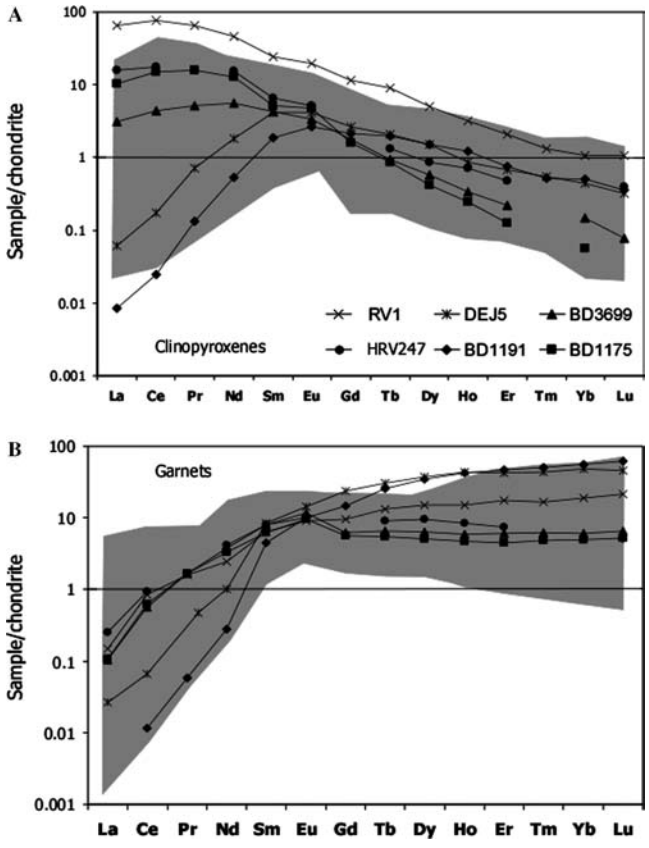

Fig. 2 Chondrite-normalized rare earth element patterns for clinopyroxene (**a**) and garnet (**b**) of the studied eclogites compared to those from eclogite xenoliths from kimberlites worldwide (grey field, Jacob 2004). Data for HRV247 from Harte and Kirkley (1997)

from eclogitic xenoliths worldwide, whereas the coexisting garnet, as in those of other samples in this suite, overlaps with the field for eclogitic garnets from our worldwide database (Fig. 2b). Only few clinopyroxenes from eclogite xenoliths show LREE of more than 30 times chondritic and only one sample (from the Bellsbank kimberlite in South Africa, not shown) is known to have La-concentrations of >100 times chondritic (Taylor and Neal 1989).

Garnets and reconstructed bulk samples BD1175 and BD3699 have pronounced positive Eu-anomalies and flat HREE patterns (Figs. 2a, 3). These are typical characteristics of eclogitic xenoliths worldwide. Often these characteristics are accompanied by positive Sr-anomalies and higher Na_2O-contents than are expected in high pressure mantle rocks. Such trace element patterns are reminiscent of plagioclase-bearing precursor rocks: they cannot be produced at high pressure, but compare very well with those of oceanic gabbros (Fig. 3).

Rutile in the very trace element depleted sample BD1191 (Table 2b) has correspondingly low concentrations of high field strength elements (HFSE) to its silicate constituents, i.e. undetectable Nb and Ta and low Zr and Hf, yielding a strongly subchondritic Zr/Hf ratio of 16 compared to a near chondritic Zr/Hf ratio of 34 for rutile in sample BD1175 (chondritic Zr/Hf = 36.3, chondritic Nb/Ta = 17.4; Sun and McDonough 1989). Rutiles in this latter sample also contain considerable Nb and Ta and show strongly subchondritic Nb/Ta ratios of 3.5. In comparison, rutiles from coesite-bearing eclogites from the same locality have Nb/Ta ratios close to the chondritic value (Jacob et al. 2003).

Isotopic systematic and ages

Hf, Nd and Sr isotopic compositions and corresponding trace element concentrations measured for minerals by isotope dilution are listed in Table 5 for minerals and are reconstructed to whole rock values in Table 6. Initial Hf isotopic ratios of cpx and garnet corrected for the age of the Roberts Victor kimberlite (128 Ma; Smith et al. 1985) are extremely heterogeneous and range between 0.281500 and 0.355077 (−42.2 to +2561 $\varepsilon_{Hf}(i)$), thus displaying both very unradiogenic as well as very radiogenic values. The large range of Hf isotopic ratios is corroborated by similarly diverse $^{143}Nd/^{144}Nd_i$ ratios between 0.511124 (−26.5 ε) and 0.545092 (+636 ε). $^{87}Sr/^{86}Sr_i$ ratios show a more restricted range and vary between 0.700888 and 0.70614. None of the samples plot in the mantle array; neither in the ε_{Hf} versus ε_{Nd} plot (Fig. 4) nor in ε_{Nd}–$^{87}Sr/^{86}Sr$ space (not shown). Such extreme values of several hundred ε-units in Nd and Hf isotopic compositions are very rare in mantle eclogites. Only garnets from eclogite xenoliths from kimberlites at Bellsbank, South Africa (Neal et al. 1990) and Udachnaya in Siberia (Pearson et al. 1995) have similar, but less extreme ε_{Nd}-values of between 100 and 200. A more extreme radiogenic Hf isotopic value of ε_{Hf} = +24,960 has been reported for an alkremite xenolith from the Udachnaya kimberlite, Siberia (garnet-spinel–bearing rock, believed to be related to the eclogitic xenolith suite; Nowell et al. 2003). Similarly low ε_{HR}-values of −41.7

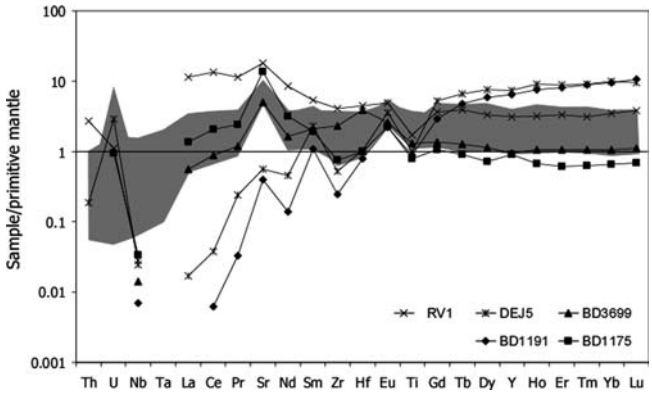

Fig. 3 Spidergram for reconstructed bulk eclogites (values from Table 4, rutile-free) normalized to values for primitive mantle compared to modern oceanic gabbros from the Indian Ocean (Bach et al. 2001)

are known from the carbonate fraction of carbonatites (Bizimis et al. 2003).

It is often suggested that the Lu–Hf isotopic system may be less susceptible to alteration effects compared to other isotopic systems, because both parent and daughter elements belong to the HREE and HFSE that are not as easily affected by metasomatic processes. This observation holds true for this study, because Nd isotopic ratios correlate with the degree of LREE enrichment (taken as a measure of metasomatic influence) in this suite of samples, whereas Hf isotopic ratios show no dependency. Almost none of samples have individual mineral phases that are in isotopic equilibrium. Clinopyroxene–garnet two point isochrons yield apparent ages from 2,760 Ma to ages in the future (Table 7). Some samples yield ages close to the kimberlite emplacement age of 128 Ma for some (but not all) of the isotopic systems (e.g. DEJ5 in Rb–Sr, BD3699 in Sm–Nd) suggesting that chemical equilibrium was achieved for these particular isotopic systems. The internal Rb–Sr age of sample BD1175 agrees with the isochron age obtained for recalculated bulk compositions (see below), whereas no geological significance can be attributed to any other apparent internal age. It should be noted that the samples reported on here do not show major element zonations nor is there significant inter-grain variability in trace element content in one sample. However, the variation of internal ages in this sample suite is representative for apparent internal ages of eclogite xenoliths from kimberlites worldwide that range from older than the age of the Earth to well into the future. Geological significance can be attributed to only a few internal ages distinct from the kimberlite emplacement age (e.g. Jagoutz 1988). In contrast, most (especially those that yield future ages) are the results of mineral disequilibrium, e.g. resulting from metamorphic growth or metasomatic overprint, whereas others are thought to represent "frozen" mineral equilibrium (Dodson 1973; see Jacob 2004 for a short summary). Reconstructed whole rock compositions of Roberts Victor eclogites yield a Sm–Nd isochron of 2,700 ± 100 Ma (Jagoutz et al. 1984) and similar late Achaean isochron ages were obtained using Pb–Pb and Re–Os isotopic systems (2,465 ± 200 Ma and > 2,500 Ma; Kramers 1979; Shirey et al. 2001). Our sample suite extends the Sm–Nd reconstructed whole-rock dataset of Jagoutz et al. (1984) and yields the same age (2,770 Ma), compared to 2,349 Ma for the Lu–Hf reconstructed whole-rock system, whereas no isochron relationship exists for the Rb–Sr reconstructed whole-rock system.

The younger Lu–Hf age for reconstructed bulk eclogites is most likely caused by re-equilibration with rutile. Some of the samples contain rutile and all calculated bulk compositions using only cpx and garnet compositions show strong depletions in Nb, Ta, Hf, Zr, Ti (Fig. 3), an indication of equilibration with rutile, even though this mineral was not observed in thin section. Rutile contributes significantly to the bulk Hf budget and has very low Lu/Hf ratios (Table 3), but its mode is difficult to estimate accurately because rutile occurs as an accessory. The effect of rutile mode on the

Table 6 Reconstructed whole rock isotopic and trace element data based on data from Tables 2 and 4

	BD 1191	BD1175	BD3699	RV 1	DEJ 5	HRV247
$^{176}Hf/^{177}Hf$ rec.	0.298849	0.282123	0.281574	0.281986	0.289914	0.282797
$^{176}Hf/^{177}Hf_i$	0.297899	0.282087	0.281547	0.281930	0.289476	0.282721
$^{176}Lu/^{177}Hf$	0.3965	0.0159	0.0114	0.0251	0.1830	0.03178
$^{143}Nd/^{144}Nd$ rec.	0.538529	0.511566	0.515434	0.511494	0.523629	0.512051
$^{143}Nd/^{144}Nd_i$	0.537302	0.511489	0.515178	0.511398	0.522889	0.511898
$^{147}Sm/^{144}Nd$	1.564	0.09804	0.3251	0.1223	0.8835	0.1818
$^{87}Sr/^{86}Sr$ rec.	–	0.701553	0.703350	0.703659	0.700928	0.705931
$^{87}Sr/^{86}Sr_i$	–	0.701521	0.703283	0.703502	0.700905	0.705923
$^{87}Rb/^{86}Sr$	0.3688	0.0184	0.0391	0.0922	1.073	0.00479
εHf_i	538	−21.6	−40.5	−27.2	240	1
εNd_i	484	−19.3	52.2	−21.1	203	−11.2
Rb rec. (ppm)	n.m.	n.m.	n.m.	n.m.	n.m.	0.0046
Nd rec. (ppm)	0.162	4.844	3.159	13.53	0.623[a]	3.643
Sr rec. (ppm)	n.m.	n.m.	n.m.	n.m.	n.m.	90.54
Sm rec. (ppm)	0.419	0.784	1.70	2.737	1.030[a]	1.096
Hf rec. (ppm)	0.237	0.4524	1.830	1.635	0.4704	0.8894
Lu rec. (ppm)	0.657	0.050	0.1458	0.2865	0.6003	0.1971

n.m. not measured
[a]Laser ablation ICP-MS data

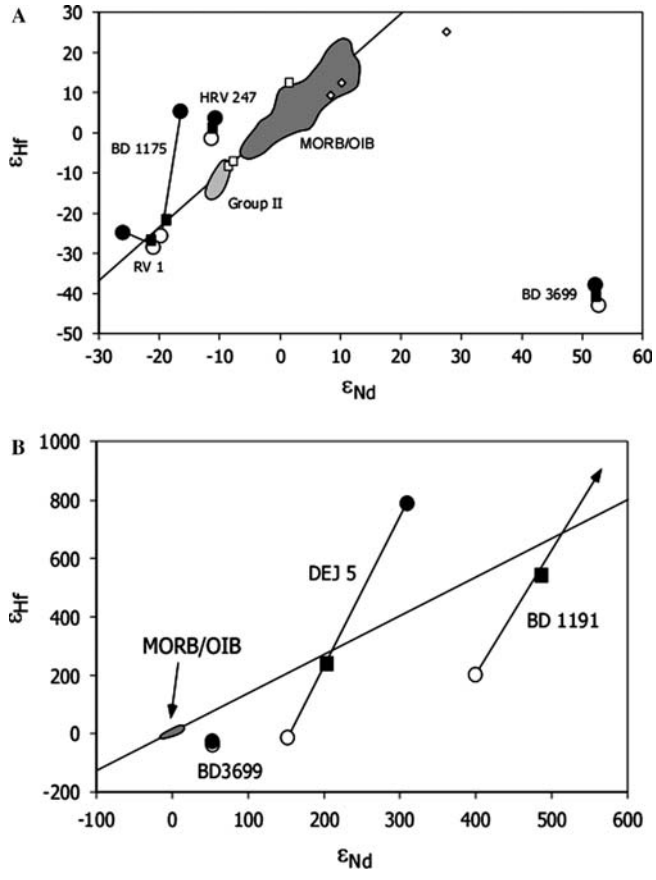

Fig. 4 Hf and Nd isotopic compositions of reconstructed eclogite bulks (*solid squares*), clinopyroxenes (*open circles*) and garnets (*solid circles*) at the time of kimberlite emplacement (128 Ma, Smith et al. 1985, recalculated with $\lambda = 1.865 \times 10^{-11}$; Scherer et al. 2001). *White diamonds* and *white squares* are bulk pyroxenites and websteritic cpx from Beni Bousera (Pearson and Nowell 2004). Field for Group 2 kimberlites (Bizimis 2001; Nowell et al. 1998), MORB-OIB field (data compiled from the literature) and terrestrial line (Vervoort et al. 1999) for reference. Figure b shows the very radiogenic eclogite samples in comparison to the MORB-OIB field and the terrestrial line

Table 7 Internal (clinopyroxene—garnet) ages of Roberts Victor eclogites uncorrected for the emplacement age of the Roberts Victor kimberlite (128 Ma, Smith et al. 1985). Hafnium ages are calculated with a decay constant of 1.865×10^{-11} (Scherer et al. 2001)

Sample	Sm–Nd age (Ma)	Lu–Hf age (Ma)	Rb–Sr age (Ma)
BD1191	907	1,400	–
BD1175	221	494	2.760
BD3699	110	394	21
RV1	−0.9	199	225
DEJ5	1.194	2.230	127
HRV247	146	23	2.210

slope of the reconstructed eclogite whole rock isochron depends on the timing of rutile formation in the rock, because the isotopic systems never completely equilibrated in the eclogites following their formation in the Archaean. If rutile formed during eclogite metamorphism (at 2.7 Ga), its present day Hf isotopic composition would be very unradiogenic and close to the initial isotopic ratio compared to that of the silicate bulk rock, because of its very low Lu/Hf ratio. Addition of unradiogenic rutile to the silicate bulk would slide the reconstructed bulk values down along the isochron towards the initial $^{176}Hf/^{177}Hf$ ratio and not affect the slope of the regression line. In this sample suite, however, there is textural as well as geochemical evidence that rutile formed later than eclogite metamorphism. In BD1191 and DEJ5 rutile is only present as needles exsolving from garnets, and concentrations of HFSE in rutile from BD1191 (Table 3) are very low, despite the minerals' very high partition coefficients for these elements. These unusually low HFSE concentrations as well as low Nb/Ta and Zr/Hf ratios show that a partial melting event affected a rutile-free bulk composition, either under amphibolite facies conditions, below the rutile stability field, or at higher pressures, deep in the upper mantle, where all TiO_2 is dissolved in cpx and garnet (Green and Sobolev 1975; Klemme et al. 2002; Konzett 1997). The low HFSE rutiles now present in these eclogites exsolved later from garnet upon cooling and decompression. In this case the effect of modal rutile on the reconstructed bulk Lu–Hf isochron is to move values to lower $^{176}Lu/^{177}Hf$ ratios and lower $^{176}Hf/^{177}Hf$ ratios, off the isochron defined by the reconstructed purely silicate bulk rock. This leads to a steeper slope of the regression line and older apparent ages of the isochrons with increasing modal rutile. This illustrates that the Lu–Hf age for reconstructed samples (pure silicates) is a minimum age and demonstrates that the Lu–Hf system is not suitable for *dating* rutile-bearing eclogite xenoliths from kimberlites via the "reconstructed whole-rock method" unless rutile modes and rutile isotopic compositions are known very accurately.

Discussion

The Hf isotopic composition of this suite of eclogite xenoliths is very heterogeneous, consistent with similarly large heterogeneities observed for the Sm–Nd and Rb–Sr isotopic systems in eclogite xenoliths worldwide. Nevertheless, Fig. 4 shows that four out of six reconstructed bulk samples plot on or very close to the extension of the terrestrial array (Vervoort et al. 1999), thus showing coupled Sm–Nd and Lu–Hf systematics. In contrast, model calculations predict a more homogeneous isotopic composition of subducted ancient MORB that should be below and much closer to the mantle array (e.g. Salters and White 1998; Pearson and Nowell 2004). This discrepancy illustrates that the complex effects of processes occurring during subduction and emplacement into the mantle are difficult to constrain by theoretical models. Furthermore, protoliths of eclogite xenoliths are more often gabbroic than basaltic, with the former showing a priori more hetero-

geneity than the latter, due to their cumulate nature. Hence, over time, small compositional heterogeneities, as well as modifications upon subduction and emplacement into the mantle (e.g. partial melting, metasomatism) lead to large heterogeneities in isotopic compositions. This suite of samples thus provides a realistic picture of ancient subducted oceanic crust.

Several authors have proposed that the "garnet-signature" as well as certain enriched characteristics of MORB and OIB may be compatible with a small percentage of subducted oceanic crust in the source (e.g. Hirschmann and Stolper 1996; Niu and Batiza 1997; Lassiter and Hauri 1998; Pertermann and Hirschmann 2003a). There are, however, several inconsistencies with the recycling hypothesis, primarily in the Pb isotopic composition of OIBs (Stracke et al. 2003). Melting experiments on eclogitic compositions (Yasuda et al. 1994; Yaxley and Green 1998; Pertermann and Hirschmann 2003a) show that for compositions with Mg-numbers of around 60, the solidus is significantly below that of peridotite implying that eclogite/pyroxenite will start melting several tens of kilometres deeper than the peridotite within an upwelling mantle (Pertermann and Hirschmann 2003b). Furthermore, eclogite solidus and liquidus are closer together in temperature than are those of peridotite so that complete melting of eclogite is established very rapidly. However, melting of a mixed peridotite/eclogite lithology is still poorly understood. Pertermann and Hirschmann (2003b) suggest that 60% of the eclogite/pyroxenite would be molten at the peridotite solidus, and that it would be completely molten at temperatures where ca. 20% of the peridotite is partially molten. Melts from such mixed sources therefore must contain high-percentage melts from the eclogite/pyroxenite "component" that would be initially tonalitic, and later basaltic in composition at higher degrees of melting (e. g. Rapp and Watson 1995). The remaining eclogite/pyroxenite restite is more refractory and therefore has a higher solidus temperature than the unmelted composition, but it is still below the peridotite solidus temperature (Irving 1974; Kogiso et al. 2003). Hence, unless melting ceases or unless it is possible to spatially separate the partial melt of eclogite/pyroxenite from its restite, 100% of the eclogite/pyroxenite will eventually contribute to the mixed peridotite-eclogite/pyroxenite melt. This also holds for cases where partial melts from eclogites impregnate peridotite (Yaxley and Green 1998), because the pyroxenite formed by the reaction of solid peridotite with eclogite melt also has a lower solidus temperature than the peridotite and, thus, will melt at lower temperatures than peridotite alone and would melt completely leaving no restite of the eclogite component.

We have modelled the possible contribution of eclogite compositions displayed by the most extreme Roberts Victor eclogites (samples RV1, BD1191, BD3699) to partial melts from spinel-peridotite (MORB source) for two cases (Fig. 5): the first case considers mixing of 60% partial melt from eclogite with 6% partial melt of spinel peridotite (dashed line in Fig. 5), following the findings of (Pertermann and Hirschmann 2003a), whereas in the second case 100% melted eclogite are mixed with 20% spinel peridotite (solid line in Fig. 5), the latter probably representing a more realistic scenario along the lines of argument above (no eclogite restite). Partial melts were calculated with the batch melting equation using partition coefficients for eclogite from Hart and Dunn (1993), Foley et al. (2000) and Johnson (1998), and from Kennedy et al. (1993) and Salters et al. (2002) for peridotite. Modes for the calculation of bulk partition coefficients were taken from Table 4 plus 0.1% rutile for eclogites and as 50% olivine, 20% opx, 20% cpx, 10% spinel for the peridotite; modelling parameters are summarized in Table 8. Figure 5 illustrates that mixing of peridotite partial melts with those from the most radiogenic eclogite (BD1191) generates compositions that rapidly move away from the MORB-OIB field at increasing eclogite/peridotite melt ratios. Mixing of 5% of the component represented by BD1191 with depleted mantle derived partial melt creates compositional shifts of 1.4 ε_{Nd} and 9.4 ε_{Hf} away from the MORB field for 100% eclogite melting (1.1 ε_{Nd} and 6.5 ε_{Hf} for 60% melting). This very radiogenic component would therefore be clearly visible in melts from a mixed source and, as MORB of such radiogenic compositions are not observed, limits its role in the basalt source regions. A similar argument holds for mixtures of melts derived from BD3699: 5% of this component mixed with partial melt from the depleted mantle shifts compositions by 1.4 ε_{Nd} to more radiogenic values and by 4.9 ε_{Hf} to less radiogenic Hf isotopic values for 100% eclogite melting (0.9 ε_{ND} and 3.4 ε_{Hf} for

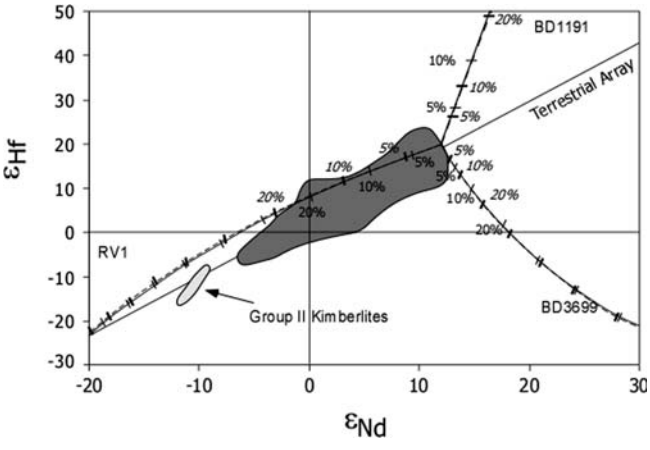

Fig. 5 Model for the potential involvement of eclogite in the production of MORB-OIB. Three exemplary eclogite samples were taken and partial batch melts of 60% eclogite were mixed with 6% partial batch melt from depleted mantle (dashed lines, fat ticks with italics giving the percentage of eclogite partial melt). *Solid lines* show results for 100% melted eclogite with 20% percent partial batch melt from depleted mantle peridotite (thin ticks). Data sources for MORB-OIB field, Group II kimberlites and terrestrial array same as in Fig. 4; modelling parameters are given in Table 8, see text for further discussion

Table 8 Modelling parameters. ε_{Hf} and ε_{Nd} for eclogite samples are present day values

	DM	DM	DM	BD1191	BD3699	RV1
Batch melt (%)		6	20	60	60	60
Nd (ppm)	0.84	8.45	3.60	0.293	3.41	17.6
Hf (ppm)	0.19	1.57	0.75	0.357	1.73	1.98
ε_{Hf}	19.4			568	−43	−29
ε_{Nd}	11.9			505	55	−22

60% melting), away from the MORB-OIB field (Fig. 5). Mixed melts derived from a component similar to RV1, however, plot within the MORB-OIB field for mixtures with up to 20% eclogite melt component (assuming 100% eclogite melting; 15% for 60% eclogite melt, Fig. 5) and could explain some of the more enriched MORB-OIB compositions.

It is important to note that the model presented here serves to illustrate the *most extreme* effects of an eclogite "component" in mixed sources for basalts for the following reasons: (1) eclogites younger than this suite have less extreme isotopic compositions and differences between their isotopic composition and that of the depleted mantle will be smaller, (2) pooling of eclogite pods in a portion of mantle during melting may average out some of the most extreme signatures, but may also lead to regionally different eclogite signatures in basalts from mixed sources, and (3) refractory eclogites with Mg-numbers >60 have solidus temperatures closer to that of peridotite (Irving 1974; Kogiso et al. 2003) and may be less melt productive yielding lower eclogite/peridotite melt ratios at the onset of melting than those proposed here that are based on the experiments of Pertermann and Hirschmann (2003b) However, we emphasize once again that it is difficult to argue for the preservation of an eclogite restite during eclogite-peridotite melting.

Conclusions

The Hf isotopic compositions of eclogitic xenoliths from kimberlites that originate from subducted oceanic crust are very heterogeneous, coherent with earlier observations for the Sm–Nd and Rb–Sr isotopic systems and are in contrast with predictions from geochemical modelling of subducted oceanic crust. Overall, the heterogeneity reflects radiogenic in-growth starting from small compositional heterogeneities in gabbroic protoliths, followed by modification during sea-floor alteration, subduction and emplacement into the subcratonic lithosphere. This suite of eclogite xenoliths therefore documents a realistic example of "aged" subducted oceanic crust.

Geochemical modelling shows that some very radiogenic isotopic compositions (displayed by sample BD1191) clearly play a limited role in MORB production; however, it should be pointed out that such extremely radiogenic compositions are rare among eclogite xenoliths from kimberlites (Jacob 2004). Other, less extreme compositions (RV1) illustrate that isotopically, up to 20% of eclogite melt may be reconcilable with the composition of some oceanic basalts.

An important observation, however, is that eclogites from the Earth's mantle are isotopically too heterogeneous to represent a "hidden reservoir" or a "component" complementary to the depleted mantle and continental crust, that is required to mass-balance the Nd and Hf isotopic composition Bulk Silicate Earth (BSE) as postulated by some authors (Blichert-Toft and Albarede 1997; Bizzarro et al. 2002).

Acknowledgements J.B. Dawson, E. Jagoutz and G. Brey are thanked for access to their Roberts Victor eclogite samples. We are also grateful to J.J. Gurney and the Kimberlite Research Group at the University of Cape Town for providing a piece of HRV247 for this study. D.J. gratefully acknowledges financial support by the DFG (Forschungsstipendium Ja 781/2). M.B. acknowledges financial support from FIU and NSF Grant OCE-0241681 to G. Sen. Reviews by H. Brueckner and S. Weyer helped to clarify some of the points stressed in this article.

Appendix

Secondary effects on whole rock Hf and Nd isotopic compositions

To constrain the effects of secondary processes on the whole rock eclogite Hf and Nd isotopic data, Hf and Nd isotopic as well as solution ICP–MS analyses of trace elements were carried out on both leached and unleached eclogite powders. Whole rock powders were leached twice with warm 2.5 N HCl for 30 min, subsequently dissolved in HF/HNO_3 and split into two aliquots. One aliquot was analysed for trace element concentrations with a Finnigan Element ICP–MS at NHMFL/FSU (see Bizimis et al. 2003; Stracke et al. 2003 for detailed analytical techniques); the other was submitted to the chemical separation scheme outlined above and measured for Hf and Nd isotopic compositions. Leachates were evaporated, re-dissolved in 2.5 N HCl and measured for their trace element concentrations by solution ICP-MS. The amount of leached material was found to vary between 6.7 and 8.6 wt% and contained 8.8–32.4% of the rock's Nd and Sm budget (Table 9). Only 3.8–7.4% of the Hf and 4.7–10.2% of the Lu budgets were in the leachates. Consistent with earlier findings (Zindler and Jagoutz 1988; Barth et al. 2001) the leachate is enriched in LILE and LREE, whereas Ti, Zr and Hf are immobile, especially in samples that contain rutile (e.g. sample DEJ5). Unleached bulk rocks have very variable isotopic compositions (grey diamonds, Fig. 6), whereas leached residues (open diamonds) converge towards the field defined by Group II kimberlites (to which the Roberts Victor kimberlite belongs) in both Nd and Hf isotopic composition, but do not agree with the reconstructed

Table 9 Isotopic composition of unleached (''bulk'') and leached samples (''residue'') compared to recalculated bulk compositions (from Table 6 and Jacob and Jagoutz 1995) and selected trace element compositions (in ppm) of unleached whole rocks (with subscript WR) and leachates (subscript L)

	RV 1	DEJ 5	HRV 247	Rovic124-A1	Rovic124-A4	BD1191
$^{143}Nd/^{144}Nd$ bulk	0.511341	n.m.	0.511937	0.512037	0.512326	0.513721
$^{143}Nd/^{144}Nd$ residue	0.511749	0.512841	0.511930	0.511966	0.512046	n.m.
$^{143}Nd/^{144}Nd$ recalc. bulk	0.511494	0.523629	0.512051	0.512902	0.512685	0.538529
$^{176}Hf/^{177}Hf$ bulk	0.281987	0.287964	0.282507	n.m.	n.m.	n.m.
$^{176}Hf/^{177}Hf$ residue	0.282217	0.287748	0.282436	n.m.	n.m.	n.m.
$^{176}Hf/^{177}Hf$ recalc. bulk	0.281986	0.289914	0.282797	–	–	–
Nd_{WR}	20.5	2.57	8.11	4.98	5.10	
Nd_L	37.8 (12.6%)	9.88 (30.6%)	30.5 (32.4%)	16.3 (26.6%)	13.3 (24.1%)	
Sm_{WR}	3.60	6.06	1.75	1.09	1.38	
Sm_L	4.59 (8.8%)	1.72 (11.8%)	4.17 (21.3%)	2.05 (15.5%)	1.76 (11.6%)	
Sr_{WR}	553	65.8	123	178	124	
Sr_L	538 (6.4%)	407 (49.4%)	331 (23.2%)	1.206 (55.3%)	568 (41.2%)	
Lu_{WR}	0.211	1.03	0.127	0.345	0.082	
Lu_L	0.165 (5.4%)	0.468 (7.3%)	0.146 (10.2%)	0.203 (4.7%)	0.056 (6.1%)	
Hf_{WR}	1.76	0.571	1.23	0.828	0.463	
Hf_L	1.18 (4.5%)	0.271 (3.8%)	1.06 (7.4%)	0.687 (6.2%)	0.367 (6.6%)	
Amount leached	6.7%	8.0%	8.6%	7.5%	8.6%	

Mass balances for leached bulk trace elements in percent are indicated in parentheses behind the leachate concentrations. Trace element concentrations were measured by solution ICP-MS at NHMFL/FSU
n.m. not measured

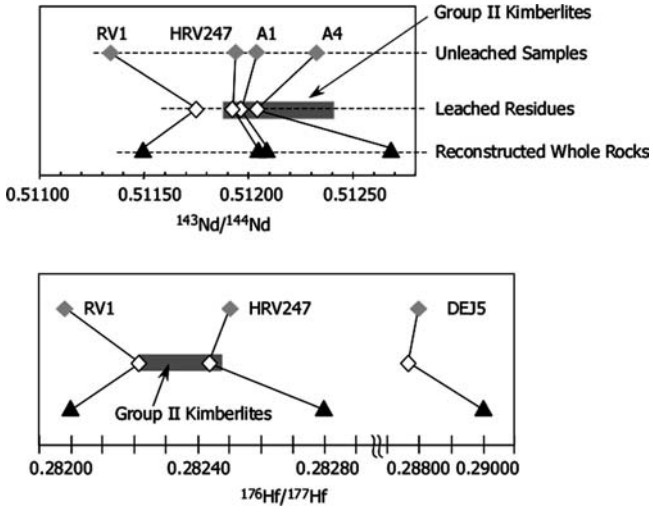

Fig. 6 Comparison of isotopic compositions of bulk eclogite samples (*grey diamonds*) with leached bulks (*white diamonds*) and reconstructed bulk compositions (*black triangles*). Acid leaching moves the isotopic compositions towards the composition of the kimberlite (*grey bar*, Smith et al. 1985). This illustrates that secondary phases are introduced into the xenoliths by infiltration and that especially interaction with the kimberlite magma leads to formation of not leachable minerals (silicates, oxides). This is consistent with findings in the literature that describe secondary phlogopite, amphibole, spinel and pyroxenes in eclogite xenoliths from kimberlites (e.g. McCormick 1994) and with comparable studies on peridotitic xenoliths from kimberlites (Richardson et al. 1985). Reconstructing the bulk via mineral analyses and modal estimations, in contrast, gives a more reliable estimate of the primary composition.

bulk compositions (black triangles). This is in agreement with the presence of both leachable and non-leachable foreign components in the eclogite xenoliths, introduced by metasomatizing fluids and deuteric alteration that have also been described from peridotitic xenolith from kimberlites (Richardson et al. 1985). These findings once again highlight the necessity to reconstruct ''clean'' bulk eclogite compositions based on mineral analyses and modes and that bulk trace element and isotopic analyses have to viewed with great caution.

References

Alt JC (1995) Subseafloor processes in mid-ocean ridge hydrothermal systems. In: Humphris SE, Zierenberg RA, Mullineaux LS, Thomson RE (eds) Seafloor hydrothermal systems: physical, chemical, biological and geological interactions. AGU, Washington, pp 85–114

Bach W, Alt JC, Niu Y, Humphris S, Erzinger J, Dick HJB (2001) The geochemical consequences of late-stage low-grade alteration of lower oceanic crust at the SW Indian ridge: results from ODP Hole 735B (Leg 176). Geochim Cosmochim Acta 65(19):3267–3288

Barth M, Rudnick RL, Horn I, McDonough WF, Spicuzza M, Valley JW, Haggerty SE (2001) Geochemistry of xenolithic eclogites from West Africa, part I: a link between low MgO eclogites and Archean crust formation. Geochim Cosmochim Acta 65:1499–1527

Barth M, Rudnick RL, Horn I, McDonough WF, Spicuzza M, Valley JW, Haggerty SE (2002) Geochemistry of xenolithic eclogites from West Africa, part II: origins of the high MgO eclogites. Geochim Cosmochim Acta 66:4325–4345

Berg GW (1968) Secondary alteration in eclogites from kimberlite pipes. Am Mineralogist 53(7–8):1336–1346

Bizimis M (2001) Geochemical processes in the upper mantle: evidence from peridotites, kimberlites and carbonatites. PhD Thesis, Florida State University, 281 pp

Bizimis M, Salters VJM, Dawson JB (2003) The brevity of carbonatite sources in the mantle: evidence from Hf isotopes. Contrib Miner Petrol 145:281–300

Bizimis M, Sen G, Salters VJM (2004) Hf–Nd isotope decoupling in the oceanic lithosphere: constraints from spinel peridotites from Oahu, Hawaii. Earth Planet Sci Lett 217:43–58

Bizzarro M, Simonetti A, Stevenson RK, David J (2002) Hf isotope evidence for a hidden mantle reservoir. Geology 30:771–774
Blichert-Toft J, Albarede F (1997) The Lu–Hf isotope geochemistry of chondrites and the evolution of the mantle–crust system. Earth Planet Sci Lett 148:243–258
Clayton RN, Goldsmith JR, Karel VJ, Mayeda TK, Newton RC (1975) Limits on the effect of pressure on isotopic fractionation. Geochim Cosmochim Acta 39:1197–1201
Dawson JB (1984) Contrasting types of upper-mantle metasomatism? In: Kornprobst J (ed) Kimberlites II: the mantle and crust-mantle relationships, vol 2. Elsevier, Amsterdam, pp 289–294
Dodson MH (1973) Closure temperature in cooling geochronological and petrological systems. Contrib Miner Petrol 40:259–274
Ellis DJ, Green DH (1979) An experimental study of the effect of Ca upon garnet-clinopyroxene Fe–Mg exchange equilibria. Contrib Miner Petrol 71:13–22
Fett A (1995) Elementverteilung zwischen Granat, Klinopyroxen und Rutil in Eklogiten—Experiment und Natur. PhD Thesis, Johannes Gutenberg Universität, Mainz
Foley SF, Barth M, Jenner GA (2000) Rutile/melt partition coefficients for trace elements and an assessment of the influence of rutile on the trace element characteristics of subduction zone magmas. Geochim Cosmochim Acta 64:933–938
Green DH, Sobolev NV (1975) Coexisting garnets and ilmenites synthesized at high pressures from pyrolite and olivine basanite and their significance for kimberlitic assemblages. Contrib Miner Petrol 50:217–229
Günther D, Longerich HP, Jackson SE (1996) A new enhanced sensitivity quadruple inductively coupled plasma-mass spectrometer (ICPMS). Can J Appl Spectrosc 40:111–116
Hart SR, Dunn T (1993) Experimental cpx/melt partitioning of 24 elements. Contrib Miner Petrol 113:1–18
Hart SR, Blusztajn J, Dick HJB, Meyer PS, Muehlenbachs K (1999) The fingerprint of seawater circulation in a 500-meter section of ocean crust gabbros. Geochim Cosmochim Acta 63:4059–4080
Harte B, Kirkley MB (1997) Partitioning of trace elements between clinopyroxene and garnet: data from mantle eclogites. Chem Geology 136:1–24
Hatton CJ (1978) The geochemistry and origin of xenoliths from the Roberts Victor mine. PhD Thesis, University of Cape Town
Hatton CJ, Gurney JJ (1979) A diamond graphite eclogite from the Roberts Victor mine. In: Proceedings of 2nd international kimberlite conference 2:29–36
Hirschmann M, Stolper E (1996) A possible role for garnet pyroxenite in the origin of the "garnet signature" in MORB. Contrib Miner Petrol 124:185–208
Hofmann AW (1988) Chemical differentiation of the Earth: the relationship between mantle, continental crust, and oceanic crust. Earth Planet Sci Lett 90:297–314
Irving AJ (1974) Geochemical and high pressure experimental studies of garnet pyroxenite and pyroxene granulite xenoliths from the Delegate basaltic pipe, Australia. J Petrol 15:1–40
Jacob DE (2004) Nature and origin of eclogite xenoliths from kimberlites. Lithos 77:295–316
Jacob DE, Foley SF (1999) Evidence for Archean ocean crust with low high field strength element signature from diamondiferous eclogite xenoliths. Lithos 48:317–336
Jacob D, Jagoutz E (1995) A diamond-graphite bearing eclogitic xenolith from Roberts Victor (South Africa): indications for petrogenesis from Pb-, Nd- and Sr- isotopes. In: Meyer HOA, Leonardos OH (eds) Kimberlites, related rocks and mantle xenoliths, vol 1. CPRM Spec Publ, Companhia de Pesquisa de Recursos Minerais, Rio de Janeiro, Brazil pp 304–317
Jacob D, Jagoutz E, Lowry D, Mattey D, Kudrjavtseva G (1994) Diamondiferous eclogites from Siberia: remnants of Archean oceanic crust. Geochim Cosmochim Acta 58:5191–5207
Jacob DE, Schmickler B, Schulze DJ (2003) Trace element geochemistry of coesite-bearing eclogites from the Roberts Victor kimberlite, Kaapvaal craton. Lithos 71:337–351
Jagoutz E (1988) Nd and Sr systematics in an eclogite xenolith from Tanzania: evidence for frozen mineral equilibria in the continental lithosphere. Geochim Cosmochim Acta 52:1285–1293
Jagoutz E, Dawson JB, Hoernes S, Spettel B, Wänke H (1984) Anorthositic oceanic crust in the Archean Earth. In: 15th lunar and planetary science conference, pp 395–396(abs)
Johnson KTM (1998) Experimental determination of partition coefficients for rare earth and high-field strength elements between clinopyroxene, garnet, and basaltic melt at high pressures. Contrib Miner Petrol 133:60–68
Kennedy AK, Lofgren GE, Wasserburg GJ (1993) An experimental study of trace element partitioning between olivine, orthopyroxene and melt in chondrules: equilibrium values and kinetic effects. Earth Planet Sci Lett 115:177–195
Klemme S, Blundy JD, Wood BJ (2002) Experimental constraints on major and trace element partitioning during partial melting of eclogite. Geochim Cosmochim Acta 66:3109–3123
Kogiso T, Hirschmann M, Frost D (2003) High-pressure partial melting of garnet pyroxenite: possible mafic lithologies in the source of ocean island basalts. Earth Planet Sci Lett 216:603–617
Konzett J (1997) Phase relations and chemistry of Ti-rich K-richterite-bearing mantle assemblages: an experimental study to 8.0 GPa in a Ti-KNCMASH system. Contrib Miner Petrol 128:385–404
Kornprobst J (1970) Les péridotites et les pyroxénites du massif ultrabasic de Beni Bouchera: une étude expérimentale entre 1100 et 1550°C sous 15 à 30 kilobars de pression sèche. Contrib Miner Petrol 29:290–309
Kramers JD (1979) Lead, uranium, strontium, potassium and rubidium in inclusion-bearing diamonds and mantle-derived xenoliths from Southern Africa. Earth Planet Sci Lett 42:58–70
Lassiter JC, Hauri EH (1998) Osmium-isotope variations in Hawaiian lavas: evidence for recycled oceanic lithosphere in the Hawaiian plume. Earth Planet Sci Lett 164(3–4):483–496
Longerich HP, Jackson SE, Günther D (1996) Laser ablation inductively coupled plasma mass spectrometric transient signal data acquisition and analyte concentration calculation. J Anal Atom Spectr 11:899–904
MacGregor ID, Manton WI (1986) Roberts Victor eclogites: ancient oceanic crust. J Geophys Res 91(B14):14063–14079
Mattey D, Lowry D, MacPherson C (1994) Oxygen isotope composition of mantle peridotite. Earth Planet Sci Lett 128:231–241
McCandless TE, Gurney JJ (1989) Sodium in garnet and potassium in clinopyroxene: criteria for classifying mantle eclogites. In: Ross J, Jaques AL, Ferguson J, Green DH, O'Reilly SY, Danchin RV, Janse AJA (eds) Kimberlites and related rocks, vol 2. GSA Special Publication No. 14, Perth, pp 827–832
McCormick TC, Smyth JR and Caporuscio FA (1994) Chemical systematics of secondary phases in mantle eclogites. In: Meyer HOA, Leonardos OH (eds) Kimberlites, related rocks and mantle xenoliths. CPRM— Special Publication. Companhia de Pesquisa de Recursos Minerais, Rio de Janeiro, Brazil, pp 405–419
Munker C, Weyer S, Scherer E, Mezger K (2001) Separation of high field strength elements (Nb, Ta, Zr, Hf) and Lu from rock samples for MC–ICPMS measurements. Geochem Geophys Geosyst 2, paper number 2001GC000183
Neal CR, Taylor LA, Davidson JP, Holden P, Halliday AN, Nixon PH, Paces JB, Clayton RN, Mayeda TK (1990) Eclogites with oceanic crustal and mantle signatures from the Bellsbank kimberlite, South Africa, part 2: Sr, Nd, and O isotope geochemistry. Earth Planet Sci Lett 99:362–379
Niu Y, Batiza R (1997) Trace element evidence from seamounts for recycled oceanic crust in the Eastern Pacific mantle. Earth Planet Sci Lett 148:471–483
Nowell GM, Kempton PD, Pearson DG (1998) Hf-Nd isotope systematics of kimberlites: relevance to terrestrial Hf-Nd systematics. Ext Abs 7th Int Kimberlite Conf, pp 628–630
Nowell GM, Pearson DG, Jacob DE, Spetsius ZV, Nixon PH, Haggerty SE (2003) The origin of alkremites and related rocks: a Lu–Hf, Rb–Sr and Sm–Nd isotope study. In: extended abstracts 8th international kimberlite conference, unpaginated

Ongley JS, Basu AR, Kyser TK (1987) Oxygen isotopes in coexisting garnets, clinopyroxenes and phlogopites of Roberts Victor eclogites: implications for petrogenesis and mantle metasomatism. Earth Planet Sci Lett 83:80–84

Pearson DG, Nowell GM (2004) Re–Os and Lu–Hf isotope constraints on the origin and age of pyroxenites from the Beni Bousera peridotite massif: implications for mixed peridotite–pyroxenite mantle sources. J Petrol 45(2):439–455

Pearson DG, Shirey SB, Carlson RW, Boyd FR, Pokhilenko NP, Shimizu N (1995) Re–Os, Sm–Nd, and Rb–Sr isotope evidence for thick Archean lithospheric mantle beneath the Siberian craton modified by multistage metasomatism. Geochim Cosmochim Acta 59:959–978

Pertermann M, Hirschmann M (2003a) Anhydrous partial melting experiments on MORB-like eclogite: phase relations, phase compositions and mineral-melt partitioning of major elements at 2–3 GPa. J Petrol 44(12):2173–2201

Pertermann M, Hirschmann M (2003b) Partial melting experiments on a MORB-like pyroxenite between 2 and 3 GPa: constraints on the presence of pyroxenite in basalt source regions form solidus location and melting rate. J Geophys Res 108. Doi 10.1029/1200JB000118

Rapp RP, Watson EB (1995) Dehydration melting of metabasalt at 8–32 kbar. Implications for continental growth and crust–mantle recycling. J Petrol 36:891–931

Richardson SH, Erlank AJ, Hart SR (1985) Kimberlite-borne garnet peridotite xenoliths from old enriched subcontinental lithosphere. Earth Planet Sci Lett 75:116–128

Rudnick RL (1995) Eclogite xenoliths: samples of Archean ocean floor. In: extended abstracts 6th international kimberlite conference, pp 473–475

Salters VJM (1994) $^{176}Hf/^{177}Hf$ determination in small samples by a high-temperature SIMS technique. Anal Chem 33:4186–4189

Salters VJM, Dick HJB (2002) Mineralogy of the mid-ocean-ridge basalt source from neodymium isotopic composition of abyssal peridotites. Nature 418:68–72

Salters VJM, Hart SR (1989) The Hf paradox and the role of garnet in the source of mid-ocean-ridge basalts. Nature 342:420–422

Salters VJM, White WM (1998) Hf isotope constraints on mantle evolution. Chem Geol 145(3–4):447–460

Salters VJM, Longhi JE, Bizimis M (2002) Near mantle solidus trace element partitioning at pressures up to 3.5 GPa. Geochem Geophys Geosyst 3(7):10.1029/2001GC000148

Scherer E, Münker C, Mezger K (2001) Calibration of the Lu–Hf clock. Science 293:683–687

Schmickler B, Jacob DE, Foley SF (2004) Eclogite xenoliths from the Kuruman kimberlites, South Africa: geochemical fingerprinting of deep subduction and cumulate processes. Lithos 75:175–207

Shirey SB, Carlson RW, Richardson SH, Menzies A, Gurney JJ, Pearson DG, Harris JW, Wiechert U (2001) Archean emplacement of eclogitic components into the lithospheric mantle during formation of the Kaapvaal craton. Geophys Res Lett 28(13):2509–2512

Smith CB, Allsopp HL, Kramers JD, Hutchinson G, Roddick JC (1985) Emplacement ages of Jurassic–Cretaceous South African kimberlites by the Rb–Sr method on phlogopite and whole-rock samples. Trans Geol Soc S Afr 88(2):249–266

Smith CB, Gurney JJ, Harris JW, Robinson DN, Shee SR, Jagoutz E (1989) Sr and Nd isotopic systematics of diamond-bearing eclogitic xenoliths and eclogite inclusions in diamond from southern Africa. In: Ross J, Jaques AL, Ferguson J, Green DH, O'Reilly SY, Danchin RV, Janse AJA (eds) Kimberlites and related rocks, vol 2. GSA Special Publication No. 14, Perth, pp 853–863

Stracke A, Salters VJM, Sims KWW (1999) Assessing the presence of garnet-pyroxenite in the mantle sources of basalts through combined hafnium–neodymium–thorium isotope systematics. Geochem Geophys Geosyst 1:paper number 1999GC000013

Stracke A, Zindler A, Salters VJM, McKenzie D, Blichert-Toft J, Albarede F, Gronvold K (2003) Theistareykir revisited. Geochem Geophys Geosyst 4:Article No. 8507

Sun S-S, McDonough WF (1989) Chemical and isotopic systematics of oceanic basalts: implications for mantle composition and processes. In: Saunders AD, Norry MJ (eds) Magmatism in the ocean basins, vol 42. Geol Soc Spec Publ, pp 313–345

Taylor LA, Neal CR (1989) Eclogites with oceanic crustal and mantle signatures from the Bellsbank kimberlite, South Africa, part I: mineralogy, petrography and whole rock chemistry. J Geol 97(5):551–567

Vervoort JD, Patchett PJ, Blichert-Toft J, Albarede F (1999) Relationships between Lu–Hf and Sm–Nd isotopic systems in the global sedimentary system. Earth Planet Sci Lett 168(1–2):79–99

Yasuda A, Fujii T, Kurita K (1994) Melting phase-relations of an anhydrous midocean ridge basalt from 3 to 20 GPa—Implications for the behavior of subducted oceanic crust in the mantle. J Geophys Res 99(B5):9401–9414

Yaxley GM, Green DH (1998) Reactions between eclogite and peridotite: mantle refertilisation by subduction of oceanic crust. Schweiz Mineral Petrogr Mitt 78:243–255

Zimmer M, Kröner A, Jochum KP, Reischmann T, Todt W (1995) The Gabal Gerf complex: a Precambrian N-MORB ophiolite in the Nubian Shield, NE Africa. Chem Geol 123:29–51

Zindler A, Jagoutz E (1988) Mantle cryptology. Geochim Cosmochim Acta 52:319–333